A mathematical model for tumor-immune dynamics in multiple myeloma: Sensitivity analysis, identifiability, and numerical simulations

Jill Gallaher, Kamila Larripa, Marissa Renardy, Blerta Shtylla, Nessy Tania, Diana White, Karen Wood, Li Zhu, Chaitali Passey, Michael Robbins, Natalie Bezman, Suresh Shelat, Hearn Jay Cho*, Helen Moore*

---

* Contributed equally to the specification of the model and the conceptual framework.

Jill Gallaher
H. Lee Moffitt Cancer Center, Tampa, FL 33612, e-mail: jill.gallaher@moffitt.org

Kamila Larripa
Department of Mathematics, Humboldt State University, Arcata, CA 95521, e-mail: kamila.larripa@humboldt.edu

Marissa Renardy
Department of Mathematics, The Ohio State University, Columbus, OH 43210, e-mail: renardy.1@osu.edu

Blerta Shtylla
Mathematics Department, Pomona College, Claremont, CA 91711, e-mail: shtyllab@pomona.edu

Nessy Tania
Department of Mathematics and Statistics, Smith College, Northampton, MA 01063, e-mail: ntania@smith.edu

Diana White
Department of Mathematics, Clarkson University, Potsdam, NY 13699, e-mail: dtwhite@clarkson.edu

Karen Wood
Department of Mathematics, University of California at Irvine, Irvine, CA 92697, e-mail: kewood@uci.edu

Li Zhu
Clinical Pharmacology and Pharmacometrics, Bristol-Myers Squibb, Princeton, NJ 08543, e-mail: li.zhu@bms.com

Chaitali Passey
Clinical Pharmacology and Pharmacometrics, Bristol-Myers Squibb, Princeton, NJ 08543, e-mail: chaitali.passey@bms.com

Michael Robbins
Hematology Medical Strategy, Bristol-Myers Squibb, Lawrence Township, NJ 08648, e-mail: michael.robbins@bms.com

Natalie Bezman
Immuno-Oncology Discovery, Bristol-Myers Squibb, Redwood City, CA 94063, e-mail: natalie.bezman@bms.com

Suresh Shelat

Abstract In this work, we analyze a mathematical model we introduced previously [29] for the in-host dynamics of multiple myeloma and the immune system. We focus on four main aspects: 1) obtaining and justifying parameter ranges and point estimates; 2) determining which parameters the model is most sensitive to; 3) determining which of the sensitive parameters can be uniquely estimated given various types of data; and 4) exploring the model and updated parameter estimates numerically. Using multiple sensitivity analysis techniques, we found that the model is generally most sensitive to parameters directly associated with M protein levels. This analysis provides the foundation for a future application of the model: prediction of optimal combination regimens in patients with multiple myeloma.

1 Introduction

Multiple myeloma (MM) is a cancer of plasma B cells. There are almost two dozen treatments approved in the US and many others currently in clinical trials [42]. Regimens usually combine multiple therapies simultaneously. Patients often receive additional different combinations, after not responding to an initial combination, or after responding and then relapsing. Many patients do not survive more than ten years [42]. Without direct comparison studies, it is difficult to know the best combinations and doses for treatment. Questions remain regarding both treatment choice and timing [42].

In this work, we use a mathematical modeling approach to address some of these challenges. A mathematical model that accurately captures important features of the disease and therapy dynamics can be used to perform *in silico* experiments that test different regimens. It can also be used to predict a regimen that is expected to perform optimally. We start with a "within-host" mathematical model of MM ("tumor") and immune system dynamics that was introduced in the work of Gallaher et al. [29]. This model includes a measure of tumor burden in a hypothetical patient with MM, along with several immune cell types that play important roles in disease control or progression. These model components and key interactions between them are included to reflect the biology and to represent targets for therapeutic intervention.

Some of the earliest mathematical models for tumor-immune system interactions include those of Stepanova [73] in 1980, Kuznetsov et al. [46] in 1994, Kirschner

Oncology Clinical Development, Bristol-Myers Squibb, Lawrence Township, NJ 08648, e-mail: suresh.shelat@bms.com

Hearn Jay Cho
Tisch Cancer Institute, Mt. Sinai School of Medicine, New York, NY 10029, e-mail: hearn.jay.cho@mssm.edu

Helen Moore
Bristol-Myers Squibb, Princeton, NJ 08543
Current address: AstraZeneca, Waltham, MA 02451, e-mail: dr.helen.moore@gmail.com

and Panetta [44] in 1998, de Vladar and González [16] and Moore and Li [54] in 2004, and d'Onofrio [22] and de Pillis et al. [15] in 2005. These models are formulated and analyzed as dynamical systems described by ordinary differential equations (ODEs) while other modeling approaches include structured population models [17], partial differential equations (PDEs) [49], cellular automata models [81], or combinations of these approaches [12]. Many of these models consist of very general descriptions of cancer dynamics, while some (e.g., the chronic myelogenous leukemia model by Moore and Li [54]) analyze tumor-immune system interactions for specific cancer types.

Our model tracks dynamics in the peripheral blood of patients with MM, although these dynamics are driven by interactions that occur elsewhere (bone marrow or lymph nodes). Levels of myeloma protein (M protein) in peripheral blood samples are strongly correlated with tumor burden [66]. Sullivan and Salmon [76] developed a simple tumor growth mathematical model in the early 1970s using M-protein levels to study chemotherapy-induced tumor regression in patients with MM. Swan and Vincent applied optimal control in 1977 [78] to predict an optimal chemotherapy dosing strategy for patients with MM. In 1977, Hokanson et al. [37] fit individual M-protein data with mathematical models that considered myeloma cell populations that were sensitive or resistant.

In 2015, Jonsson et al. [40] published a model of patient M-protein levels in response to treatment with carfilzomib (CFZ). Terms that captured the concentrations of CFZ over time were included, and were fit to individual patient data using nonlinear mixed effects modeling. A model for survival was also included, and covariates for each model were tested and found to be significant for patient survival prediction.

Tang et al. [79] published a model in 2016 for patient M-protein levels in clinical trials testing bortezomib-based chemotherapy. Although data from hundreds of patients were available and some patients had less data available than others, the model was fit to each individual separately, and parameter estimates were averaged. The model validation was performed on aggregated quartiles of M-protein levels. Their mathematical model proposed a differentiation hierarchy in the bone marrow with a myeloma progenitor cell population that might cause relapse. They predicted that rational combination treatments with decreased selection pressure on myeloma cells could lead to a longer remission period.

In 2017, Nanavati et al. [55] published a semi-mechanistic protein production and signaling model with seven main compartments. Additional compartments were used to represent the concentration of the treatment vorinostat and as "transit" compartments to introduce delays into the model. The model was fit to aggregate *in vivo* xenograft data (digitized from the literature) for mice treated with vorinostat.

These prior studies have not examined the role of the immune system in MM disease dynamics. Several immunomodulatory drugs have been approved for use in MM, and more are currently in clinical trials [42]. As we plan to eventually optimize regimens for patients with MM and include immunotherapies, our model includes key tumor-immune interactions in patients with MM.

Our mathematical model consists of a dynamical system that tracks a tumor burden marker and several immune cell components. We track the level of M protein in the peripheral blood, which we consider to be a surrogate of tumor burden in patients with MM [24]. The immune cells included in our model are cytotoxic T lymphocytes, natural killer cells, and regulatory T cells.

In this paper, we carefully justify ranges and values of parameters in the model from the literature. Based on these ranges, we perform global sensitivity analyses to determine the parameters of the model with the largest effect on the outcomes. We look for improved estimates of these sensitive parameters by fixing the other parameters, and fitting the model to aggregate data in the literature. With these updated parameter estimates, we determine identifiability of the sensitive parameters assuming the availability of additional data. Finally, we explore the full model with numerical simulations.

By determining sensitive parameters in the model, we have the potential to reduce the complexity of the model. We can fix the insensitive parameters to estimated values, and only allow the sensitive parameters to vary between hypothetical subjects. This simpler model can be used in the future to predict optimal combination regimens *in silico*. These predictions can then be tested either preclinically or clinically and compared to regimens with known outcomes to evaluate and calibrate the results.

2 The Mathematical Model

Our mathematical model, originally presented in [29], consists of a system of ordinary differential equations which represent interactions between myeloma cells and the immune system. We include the following four populations in the peripheral blood: M protein produced by MM cells, $M(t)$; natural killer (NK) cells, $N(t)$; cytotoxic T lymphocytes (CTLs), $T_C(t)$; and regulatory T cells (Tregs), $T_R(t)$. A detailed description and justification of the model interactions is given in [29]. The interactions between the populations are represented in Fig. 1 and summarized in Table 1.

The model equations (1) – (4) are given below, with the labels $a-k$ above the corresponding interactions described in Table 1.

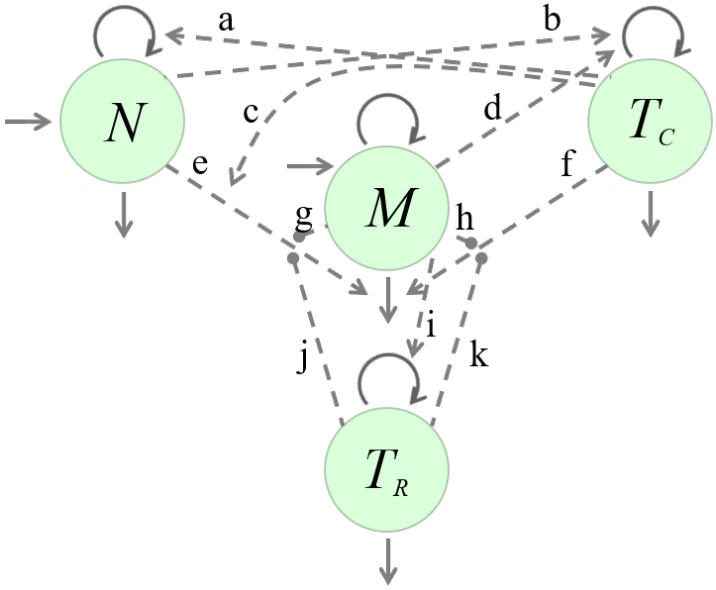

Figure 1 Diagram of population interactions. M represents M protein produced by MM cells, T_C represents CTLs, N represents NK cells, and T_R represents Tregs. The solid curves represent an increase (arrows pointing in) or decrease (arrows only pointing out) in population sizes. The dashed curves represent interactions that either boost (arrows) or inhibit (solid circles) population sizes or rates of change. These interactions (labeled **a - k**) are summarized in Table 1.

Label	Interaction	References
a	T_C crosstalk with N; boosts N proliferation	[6], [48], [52], [67], [68], [70]
b	N crosstalk with T_C; boosts T_C proliferation	[6], [58], [67]
c	T_C increases activation/efficacy of N cells	[48], [52], [68]
d	Antigens shed from M stimulate T_C proliferation	[1], [18], [23], [39], [63], [84]
e	N cells kill myeloma cells	[8], [9], [19], [28], [41], [62]
f	T_C cells kill myeloma cells	[19], [41], [84]
g	Myeloma cells decrease efficacy of N cells	[30]
h	Myeloma cells decrease efficacy of T_C cells	[7], [13], [26], [64], [75]
i	Myeloma cells help T_R cells proliferate	[13], [25], [27], [26]
j	T_R decreases efficacy of N cells	[31], [32], [43], [71], [77], [80]
k	T_R decreases efficacy of T_C cells	[10], [21], [43], [51], [69], [80]

Table 1 Description of interactions between populations in the model.

$$\frac{dM}{dt} = s_M + r_M\left(1-\frac{M}{K_M}\right)M$$
$$-\delta_M\left[1+\left(\overbrace{\frac{a_{NM}N}{b_{NM}+N}}^{e}+\overbrace{\frac{a_{CM}T_C}{b_{CM}+T_C}}^{f}+\overbrace{a_{CNM}\frac{N}{b_{NM}+N}\cdot\frac{T_C}{b_{CM}+T_C}}^{c}\right)\cdot \quad (1)$$
$$\left(1-\overbrace{\frac{a_{MM}M}{b_{MM}+M}}^{g,h}-\overbrace{\frac{a_{RM}T_R}{b_{RM}+T_R}}^{j,k}\right)\Bigg]\cdot M$$

$$\frac{dT_C}{dt} = r_C\left(1-\frac{T_C}{K_C}\right)\left(1+\overbrace{\frac{a_{MC}M}{b_{MC}+M}}^{d}+\overbrace{\frac{a_{NC}N}{b_{NC}+N}}^{b}\right)T_C-\delta_C T_C. \quad (2)$$

$$\frac{dN}{dt} = s_N + r_N\left(1-\frac{N}{K_N}\right)\overbrace{\left(1+\frac{a_{CN}T_C}{b_{CN}+T_C}\right)}^{a}N-\delta_N N \quad (3)$$

$$\frac{dT_R}{dt} = r_R\left(1-\frac{T_R}{K_R}\right)\overbrace{\left(1+\frac{a_{MR}M}{b_{MR}+M}\right)}^{i}T_R-\delta_R T_R \quad (4)$$

In the absence of the others, each population is assumed to grow logistically (with growth rates denoted by r_i), and decay exponentially (with death rates defined by δ_i).

Equation (1) describes the dynamics of the myeloma cell population, represented by the concentration of M protein in the blood. The population growth includes a constant source term, representing production of protein of similar weight from sources other than myeloma cells [20].

The nonlinear term multiplying the death rate constant δ_M describes how this death rate can be increased or decreased, depending on the cell-cell interactions. In particular, the first part of the nonlinear term indicates that NK cells (N) and CTLs (T_C) kill myeloma cells (e and f respectively), and that the crosstalk between NK cells and CTLs (c) further increases the efficacy of NK killing of myeloma cells.

However, M protein (M) and Tregs (T_R) decrease the efficacy of NK and CTL killing of myeloma (g, h, j, and k). We use saturating functional forms for feedback (rather than mass action) so that there is a limit to the size of each possible effect.

Equation (2) describes the dynamics of the CTL population. The growth (proliferation) of CTLs is increased by the presence of MM and NKs (b and d, respectively). Finally, the equations (3) and (4) describe the dynamics of NKs and Tregs, respectively. NK cell proliferation is increased by crosstalk with CTLs (a), and Treg proliferation is increased through activation by MM cells (i).

3 Parameter Values and Ranges

In this section, we summarize literature information related to parameters in our model, and explain our decisions for parameter values and ranges that we used.

Growth and decay parameters for M protein, M

Normal plasma cells produce immunoglobulin (Ig), which has multiple types. A patient with MM typically overproduces one immunoglobulin type, with the majority of patients overproducing IgG and most other patients overproducing IgA [47]. We used values associated with IgG whenever a choice must be made for patients with MM [35, 79].

Constant source term, s_M: In healthy adults, a typical level of IgG in the peripheral blood is approximately 1 g/dL [34, 60, 74, 82]. In the absence of myeloma ($r_M = 0$ in healthy cases), we reduced Equation (1) to $dM/dt = s_M - \delta_M M$. Using $\delta_M = 0.001$/day (the low end of the range determined in the δ_M section below) and a steady-state value of $M_{ss} = 1$g/dL yields $s_M = 0.001$ g/dL·day. The s_M term is the only term in our model that is not related to multiple myeloma. Additionally, the model is only sensitive to it when levels of M are close to 1 g/dL (from global sensitivity analysis not shown). Thus we fixed s_M to a value of 0.001 g/dL·day, as we restricted our model to patients with multiple myeloma.

Growth rate constant, r_M: The mathematical model of Jonsson et al. [40] of M protein levels for multiple myeloma patients lists an M-protein growth rate constant of 0.0283/week $\approx$ 0.004/day, which corresponds to a doubling time of $\ln(2)/0.004 \approx 173$ days.

In Nardiello et al. [56], a plasma cell proliferation index (PCPI) assay was used to determine the fraction of cells undergoing proliferation in multiple myeloma cell samples from the bone marrow of patients. Due to the design of the PCPI assay, which measures the proliferation marker Ki-67 in cells, the resulting values are over-estimates. The lowest value in that work was 6.9%, which was for the group of newly-diagnosed patients. Kumar et al. [45] used BrdU to assess proliferation of myeloma cells from patients (as a percentage of cells entering S phase during the incubation time). The labeled cells had median values of 0.4% and 1.2% in samples from peripheral blood and bone marrow, respectively. Considering the results of both the PCPI and BrdU assays, we used a value of 3.5% of cells initiating proliferation over two days, giving a rate constant of 0.0175/day.

We also considered growth rate values from several mathematical models of tumor and immune cell interactions that are not specific to multiple myeloma. Arciero et al. [2] used a growth rate value of $r = 0.18$/day to represent growth of an aggressive tumor (doubling time of 3.85 days). De Pillis et al. [15] used a tumor growth rate of 0.51/day based on mouse data from [19]. Thus, we used a parameter range of 0.004-0.5/day for r_M.

Decay rate constant, δ_M: Hansen et al. [36] estimated the half-life of M protein to be 11.9 days ($\delta_M = 0.058$/day). Mills et al. [53] cited the following half-life values for M protein: 21-25 days for IgG subtype and 7-14 days for IgA subtype (rates of 0.028-0.099/day). However, both of these studies were of patients who had received treatment that should contribute to the loss rate of M protein, so the cited half-lives are not due to δ_M alone. Moreover, in our equation for M, we also have several immune interactions contributing to loss of M, which we expect would be reflected in the half-lives cited above. Thus δ_M would be lower than if it were the only contribution to the half-lives cited above. If we assume Equation (1) is in steady state, and if we use values shown in Table 2 for parameters other than δ_M, then we get a value between 0.001 and 0.002 for δ_M. We chose a range of 0.001-0.1/day for δ_M, and a value of 0.002.

Carrying capacity, K_M: Among 10,750 patients characterized in Greipp et al. [35], the median M-protein level was 3.9 g/dL. A similar range was also observed in Tang et al. [79] prior to treatment. Anecdotally, there are reports of values higher than 10 g/dL. We chose a range of 7-15 g/dL for the carrying capacity.

Growth and decay parameters for CTLs, T_C

Growth rate constant, r_C: De Boer et al. [5] fit a differential equation model to data to characterize immune response during viral infection (lymphocytic choriomeningitis). They found that CD8+ cells have a biphasic response: an initial expansion phase with doubling time of 8 hours followed by a contraction phase with a half-life of 41 hours. The initial doubling time translates to a growth rate of $r_C \approx 2.31$/days. We used this fast rate (stimulated response) as an upper bound for r_C. A mathematical model of tumor and immune response by Arciero et al. [2] used a sigmoidal dependence for effector cell proliferation (dependent on TGF-β both for immune suppression and stimulation) with a maximum proliferation rate of 0.1245/days. De Pillis et al. [14] estimated that the rate of CD8+ T cell activation induced by IL-2 is 1.11/day in a model of immune response for renal cell carcinoma. A mathematical model by de Boer et al. of T-lymphocyte anti-tumor response used a doubling time of 16 hours (rate of 1.04/day) for activated T cells [4]. We chose a parameter range of 0.01-0.5/day, which is slightly lower than the higher values cited, as r_C reflects the regular proliferation rate for CTL, with additional activation by myeloma and NK cells controlled by the parameters a_{MC}, b_{MC}, a_{NC}, and b_{NC}.

Carrying capacity, K_C: Using data presented in Pessoa et al. [59], we estimated that CTL populations can reach levels as high as 1500 cells/μL in MM patients, particularly in patients with long-term disease control. Thus, we chose 600-1500 cells/μL for the range of values considered for the carrying capacity K_C.

Decay rate constant, δ_C: Using a half-life value of 41 hours during a contraction phase of a viral infection as in De Boer et al. [5], the decay rate would be 0.405/day. Sontag [72] used a decay rate of 0.1/day. However, slower rates have also been used. Arciero et al. [2] gave a decay rate of 0.03/day for effector cells. De Boer et al. [4]

gave a turnover time for T lymphocyte of 50 days (rate of 0.014.day). De Pillis et al. [14] cited that for healthy donors, CD8+ cells have a half-life of 77 days which translates to a rate of 0.009/day (parameter m in their work). We thus considered a range of 0.01-0.5/day for δ_C.

Growth and decay parameters for NK cells, N

Constant source term, s_N: The source term s_N is included in our model because we expect the innate immune system to have non-negligible production of NK cells with efficacy against myeloma cells. de Pillis et al [15] used a constant source term of 1.3×10^4 cells/day for NK population dynamics. Dividing by a typical total blood volume of 5L for an adult, this results in 0.0026 cells/μL/day. Zhang et al. [85] gave a production rate of $\sim 14 \times 10^6$ cells/L/day for healthy subjects and $\sim 7 \times 10^6$ cells/L/day ($7 - 14$ cells/μL/day). We chose a parameter range of 0.001-5 cells/μL/day.

Growth rate constant, r_N: An *in vivo* study of NK cells from healthy subjects found a doubling time of 16 days in healthy young adults (rate of 0.04/day), but a slower rate of 0.02/day (doubling time of 28 days) in healthy elderly subjects [85]. de Pillis et al. used a maximal rate of 0.5/day for NK cell recruitment by tumor cells [15], and another of their models gave a value of 0.0668/day for the maximum rate of NK cell proliferation induced by IL-2 [14]. We chose a parameter range of 0.01-0.5/day for r_N.

Carrying capacity, K_N: Based on the higher range of observed values of ~ 600 cells/μL among MM patients [59], we chose a range of 300-650 cells/μL for the carrying capacity K_N.

Decay rate constant, δ_N: The *in vivo* studies of Zhang et al. [85] gave half-lives of 10 or 11 days (mean for healthy elderly and healthy young adults, respectively) which translates to a decay rate constant of 0.06-0.07/day. The model in [14] used a turnover rate of 0.0125/day for NK cells, and the model in [15] used a turnover rate of 0.0412/day. We chose a parameter range of 0.01-0.5/day.

Growth and decay parameters for Tregs, T_R

Growth rate constant, r_R: Vukmanovic-Stejic et al. [83] assayed human samples and found that Tregs have a typical proliferation rate of 0.0831 cells/μL * day. Similar to ranges we used for growth/decay rates for other immune cells, we considered a range of 0.01-0.5/day for r_R.

Carrying capacity, K_R: The high range of Tregs seen in [59] is ~ 100 cells/μL. We then use a range of $60 - 120$ cells/μL for K_R.

Decay rate constant, δ_R: Vukmanovic-Stejic et al. [83] also studied the turnover rates of Tregs. They found a turnover or loss rate constant of 0.0658/day. A math-

ematical model of tumor-immune interaction [65] used a decay rate of 0.1/day for the Tregs population. We thus considered a range of 0.01-0.5/day

Hill function parameters for feedback terms

We allowed most of the a_{ij} to vary from 0-10, i.e., from no change to more than an order of magnitude increase in respective death and growth rates, depending on their function. We considered a slightly wider range for a_{NM}, a_{CM} and a_{CNM}, reflecting a high killing efficacy by immune cells. We restricted $a_{MM} + a_{RM} \leq 1$ to ensure the correct sign for the loss rate for M. We allowed the threshold values, b_{ij}, to vary between 0 to 2 times the respective carrying capacity. For point estimates of the b_{ij}, we chose values below half the respective carrying capacity.

Parameter Table

Index	Name	Description	Range Considered	References	Used	Bistable
-	s_M	Constant source for M	0.001 g/dL·day	[34, 36, 53, 60, 74, 82]	0.001	0.001
1	r_M	Proliferation rate constant for M	0.004-0.5/day	[2, 15, 40]	0.0175	0.025
2	K_M	Carrying capacity for M	7-15 g/dL	[59]	10	13
3	δ_M	Basal death/decay rate constant for M	0.001-0.1/day	[36, 53]	0.002	0.007
4	a_{NM}	Maximum fold-increase in death rate of M by N	0-20	Estimated	5	5
5	b_{NM}	Threshold for increase in death rate of M by N	0-650	Estimated	150	275
6	a_{CM}	Maximum fold-increase in death rate of M by T_C	0-20	Estimated	5	5
7	b_{CM}	Threshold for increase in death rate of M by T_C	0-1500	Estimated	375	500
8	a_{CNM}	Maximum fold-increase in N efficacy from T_C	0-20	Estimated	8	10
9	a_{MM}	Maximum extent M decreases T_C and N efficacy	$a_{MM}+a_{RM}\leq 1$	Estimated	0.5	0.35
10	b_{MM}	Threshold for M decreasing T_C and N efficacy	0-15	Estimated	3	1.56
11	a_{RM}	Maximum extent T_R decreases T_C and N efficacy	$a_{MM}+a_{RM}\leq 1$	Estimated	0.5	0.64
12	b_{RM}	Threshold for T_R decreasing T_C and N efficacy	0-120	Estimated	25	10
13	r_C	Proliferation/activation rate constant for T_C	0.01-0.5/day	[2, 4, 5, 14]	0.013	0.45
14	K_C	Carrying capacity for T_C	600-1500 cells/μL	[59]	800	1000
15	δ_C	Death/inactivation rate constant for T_C	0.01-0.5/day	[2, 4, 5, 14, 72]	0.02	0.35
16	a_{MC}	Maximum fold-increase in activation rate of T_C by M	0-10	Estimated	5	1
17	b_{MC}	Threshold for increase in activation rate of T_C by M	0-15	Estimated	3	6.5
18	a_{NC}	Maximum fold-increase in activation rate of T_C by N	0-10	Estimated	1	1
19	b_{NC}	Threshold for increase in activation rate of T_C by N	0-650	Estimated	150	275
20	s_N	Constant source rate for N	0.001-5 cells/μL·day	[15, 85]	0.03	1.49
21	r_N	Proliferation rate constant for N	0.01-0.5/day	[14, 15, 85]	0.04	0.02
22	K_N	Carrying capacity for N	300-650 cells/μL	[59]	450	550
23	δ_N	Basal death/inactivation rate constant for N	0.01-0.5/day	[14, 15, 85]	0.025	0.025
24	a_{CN}	Maximum fold-increase in activation rate of N by T_C	0-10	Estimated	1	1
25	b_{CN}	Threshold for increase in activation rate of N by T_C	0-1500	Estimated	375	375
26	r_R	Proliferation/activation rate constant for T_R	0.01-0.5 cells/μL·day	[83]	0.0831	0.1
27	K_R	Carrying capacity for T_R	60-120 cells/μL	[59]	80	100
28	δ_R	Basal death/inactivation rate constant for T_R	0.01-0.5/day	[65, 83]	0.0757	0.077
29	a_{MR}	Maximum fold-increase in activation rate of T_R by M	0-10	Estimated	2	1
30	b_{MR}	Threshold for increase in activation rate of T_R by M	0-15	Estimated	3	3.25
31	M^0	Observed values of M protein in diseased state	0.5 - 10 g/dL	[35, 47, 79]	4	1.92 or 0.96
32	T_C^0	Observed values of CTL in diseased state	464 ± 416 cells/μL	[59]	464	464
33	N^0	Observed values of NK in diseased state	227 ± 141 cells/μL	[59]	227	227
34	T_R^0	Observed values of T_R in diseased state	42 ± 26 cells/μL	[59]	42	42

Table 2 Table of parameter descriptions and ranges of values used in the model. All parameters are assumed non-negative. M^0, T_C^0, N^0, T_R^0 are used as initial values/conditions.

4 Numerical Simulations

In this section, we use numerical simulation to explore the behavior of our model system. In Section 4.1, we focus on steady-state behavior, and provide plots of example trajectories for the solutions to Equations (1)-(4). For collections of sampled parameter sets, we show a distribution of the populations' steady-state values, and a distribution of times needed for M to reach steady state. In Section 4.2, we illustrate an example of model bistability. That is, for a given set of model parameters, we show how small perturbations in initial M-protein levels can lead to either high

M-protein level, or low M-protein level. Finally, in Section 4.3, we examine differences between high and low M-protein states. For the parameter sets sampled previously, we plot the distribution of each population size, separated by high and low M-protein states. We also plot the distributions of sizes of each net killing effect defined by the labeled terms in Equation (1), separated by high and low M-protein states.

4.1 Steady-state results

Simulation results using the specific parameter values listed in the Used column of Table 2 are shown in Fig. 2. We also plotted the histogram of steady-state values of the model variables when we simulated 10,000 sets of parameter values chosen from the range listed in in Table 2. The distribution of steady-state values is consistent with observations in the literature [35, 79, 59].

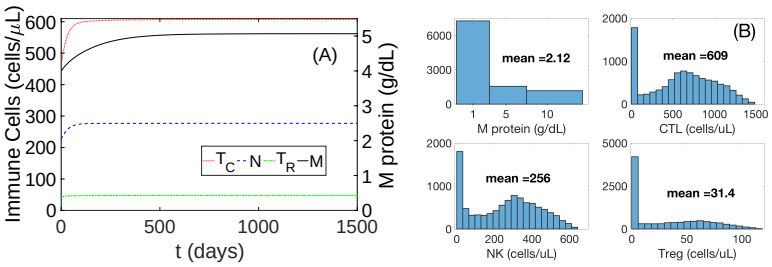

Figure 2 Baseline simulation results using parameter values listed in Table 2. **(A):** Dynamics of model variables using parameter values and initial conditions listed on the Used column in Table 2. **(B):** Histograms of steady-state values of model variables obtained from simulating the model for $0 \leq t \leq 1000$ days using 10,000 sets of parameter values sampled from the range listed on the Range Considered column in Table 2 (parameter sampling was done using Latin Hypercube sampling, see Sensitivity Analysis section further on).

Figure 3 shows a histogram of the times to steady state (log scale), normalized so that the total area is equal to 1. Out of all 10^4 samples, 77.7% reached steady state within one year, 53.8% reached steady state within 6 months, 23.7% reached steady state within 3 months, and less than 0.1% reached steady state within one month. On a log scale, the distribution is unimodal with median 146 days and mean 165 days.

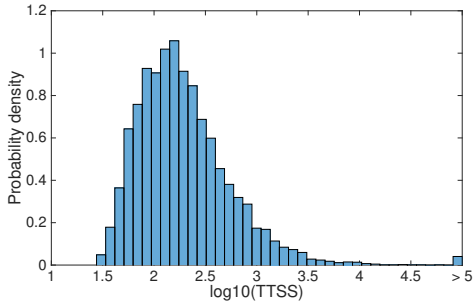

Figure 3 Histogram of times to steady state for 10^4 simulations. Time is measured in days and is presented on a log scale.

4.2 Numerical bistability

To illustrate other types of qualitative behavior that our model exhibits, aside from the baseline simulations displayed in Figure 2, we show an example of model bistability. Similar bistable results were identified for a reduced version of the model (1) through (4), where NKs and Tregs are held fixed [29]. Here we simulate the full non-scaled model (1) through (4). Parameter values used in the simulation of the model are recorded in Table 2.

Figure 4 illustrates the model's bistable behavior. The left figure corresponds to high tumor burden (achieved for a larger M initial condition), while the right figure represents a state of disease control (achieved for a smaller M initial condition). The scale to the left of each figure corresponds to immune cell concentrations (T_C, N and T_R), while the scale to the right of each figure corresponds to M-protein concentration (the solid black curves represent the M-protein concentration over time). Here, we note that the steady-state value for M in the case of higher tumor burden is 3.37 g/dL, and is 0.16 g/dL for disease control.

For each simulation, we initialize our model using immune cell counts that correspond to a diseased state ($T_C(0) = 464, N(0) = 227, T_R(0) = 42$) [59]. For a healthy individual, M-protein is approximately ≤ 1 g/dL [74].

In Figure 4 (left), we initialize the M-protein to a value of 1.92 g/dL. In this case, we note an immune response, where both NK and CTL populations increase (although, NK cells increase only marginally). However, this immune response is not enough to lower the tumor burden. Here, the steady-state value for M-protein is high (3.37 g/L), and the steady-state values for the immune cell populations are 567.40, 231.17, and 48.98 cells/μL for CTLs, NKs, and Tregs, respectively.

In Figure 4 (right), we initialize an M-protein level of 0.96 g/dL. Here we note an initial immune response, where CTL populations increase slightly. The NK cell population remains near constant, and Treg population decreases. As the M-protein levels progressively decrease to a state of disease control (steady-state value of M-protein 0.16 g/L), the immune response is suppressed (described by a drop in CTL

population). The steady-state values for the immune cell populations are 472.40, 225.06, and 26.46 cells/μL for CTLs, NKs, and Tregs, respectively.

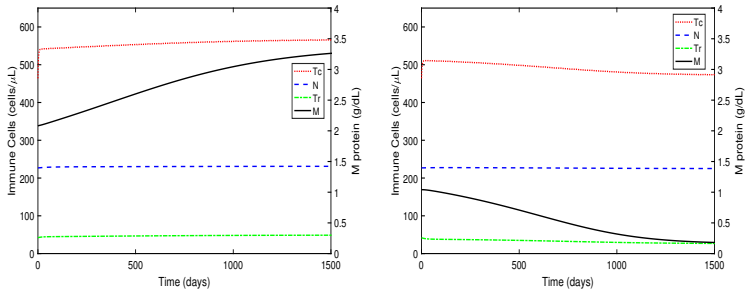

Figure 4 Initial condition for MM is varied. Initial conditions, corresponding to a diseased state [59], are held fixed are $T_C(0) = 464, N(0) = 227, T_R(0) = 42$. Scale to left corresponds to immune cells T_C, N, and T_R , and scale to the right corresponds to M-protein concentration (illustrated by solid black line). **Left:** $M(0) = 1.96$. Final M-protein level is 3.37 ($K_M = 13$). **Right**: $M(0) = 0.96$. Final M- protein level is 0.16. Other parameter values are: $r_M = 0.025$, $\delta_M = 0.007$, $s_M = 0.001$, $r_C = 0.45$, $\delta_C = 0.35$, $r_N = 0.02$, $\delta_N = 0.025$, $s_N = 1.49$, $r_R = 0.1$, $\delta_R = 0.077$. $b_{NM} = 0.5 * K_N$, $b_{CM} = 0.5 * K_C$, $b_{MM} = 0.12 * K_M$, $b_{RM} = 0.1 * K_R$, $b_{MC} = 0.5 * K_M$, $b_{NC} = 0.5 * K_N$, $b_{CN} = 0.375 * K_C$, $b_{MR} = 0.25 * K_M$, $a_{NM} = 5$, $a_{CM} = 5$, $a_{CNM} = 10$, $a_{MM} = 0.35$, $a_{RM} = 0.64$, $a_{MC} = 1$, $a_{NC} = 1$, $a_{CN} = 1$, $a_{MR} = 1$. The carrying capacities are: $K_M = 13$, $K_C = 1000$, $K_N = 550$, and $K_R = 100$.

4.3 Distinctions between high and low M protein cases

Next, we wished to sort the different immune populations outcomes produced by the model as parameter values were simultaneously varied (using 10,000 sets of parameters). Specifically, we classified the model outcomes into two categories based on long-term M protein levels: 1) low M protein levels (i.e., $M \leq 3$ g/dL), 2) high M protein levels (i.e., $M > 3$ g/dL). Our motivation for this was that data from Pessoa et al [59] showed that long term disease control patients with multiple myeloma had a particular immune signature corresponding to high average CTL counts and slight variations in average NK and Treg cell counts as compared to fully symptomatic MM patients. In other words, here we sought to analyze the pathway by which our model could produce either high or low M proteins and compare it with the data.

In Figure 5-(A), we showed box plots of steady state values. Simulations from 10,000 sampled parameter values showed that differences between low and high M can be distinguished by higher v.s. lower NK population respectively, and lower v.s. higher Treg population respectively. However, CTL population size remained relatively similar. This is contrast to data shown in [59] which showed a much higher CD8+ immune population for patients with long-term diseased control (however, when all effector T cells, CD4+ and and CD8+, were combined, the differences

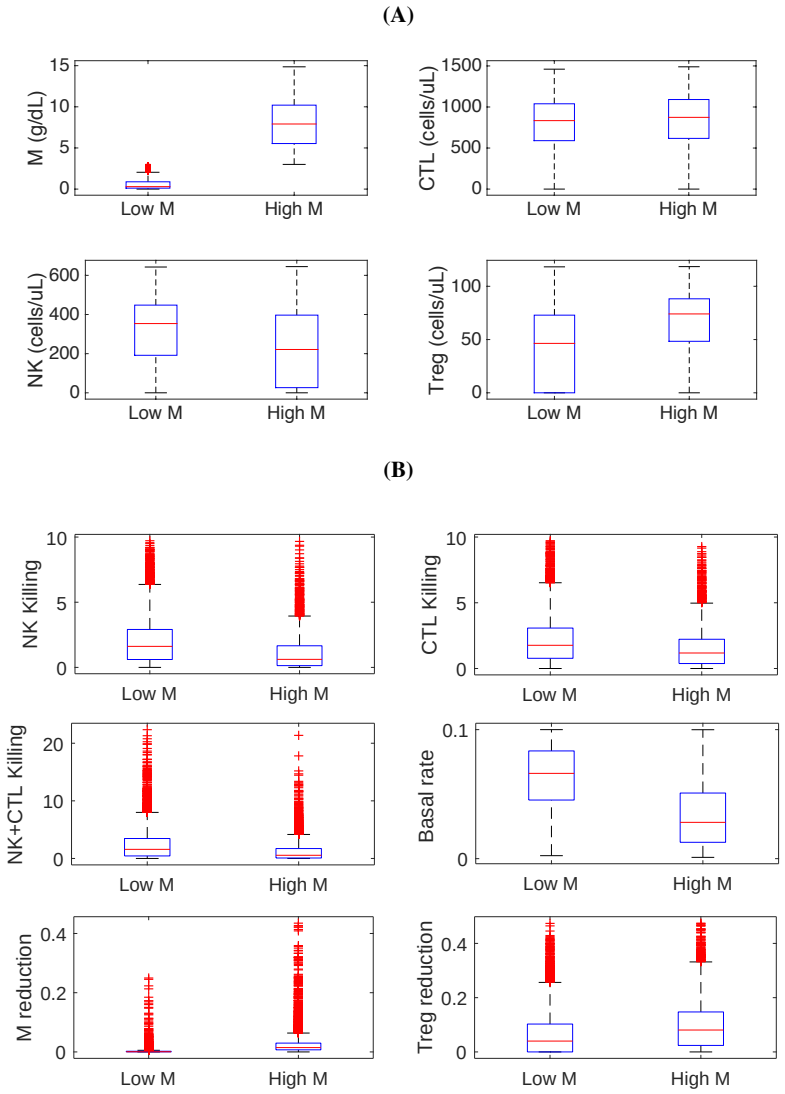

Figure 5 Comparison between long term Low M protein and High M protein. **(A):** Box plots of steady-state values. **(B):** Box plots of size of myeloma killing terms as used in (1): NK Killing: $(a_{NM}N)/(b_{NM}+N)$, CTL Killing: $(a_{CM}T_C)/(b_{CM}+T_C)$, NK+CTL Killing: $(a_{CNM}\cdot T_C\cdot N)/((b_{NM}+N)\cdot(b_{CM}+T_C)$, Basal kill rate δ_M, Kill Reduction by M: $(a_{MM}M)/(b_{MM}+M)$, Kill Reduction by Treg: $(a_{RM}T_R)/(b_{RM}+T_R)$. Steady state values of variables were used to compute killing terms. Model simulation was performed for $0 \le t \le 1200$ days using 50,000 sets of parameter values sampled from the range listed on the Range Considered column in Table 2 (parameter sampling was done using Latin Hypercube sampling, see Sensitivity Analysis section further on).

between patients with long term control and those with poor outcome were not as prominent). However, the steady-state values in our model may not fully reflect the true efficiency of immune cells in keeping the myeloma population in-check (since all parameter values were changed during sampling, including a_{ij} and b_{ij} values reflecting feedback). Hence, we next computed the size of the killing efficiency terms as defined in (1) as shown in Fig. 5-(B). Here, we saw that killing efficiencies by both NK and CTL were higher, on average, for the Low M-protein case indicating that both immune populations contributed in killing myeloma cells in agreement with the results shown in [59]. Interestingly, we saw a slightly higher CTL steady-state values for the Low M-protein case when we also performed simulations where we fixed the feedback killing efficiency parameters (all a_{ij} and b_{ij} were set to the values in the Used column in Table 2 instead of sampled from a range; figure not shown). In conclusion, results from our model suggest that while CTL contributed slightly in lowering M-protein level, the primary mechanisms for controlling myeloma level were due to an increase in NK and a decrease in Treg populations.

5 Sensitivity Analysis

Due to the high levels of uncertainty and variability in the model parameter values, we performed sensitivity analysis to determine if some of the parameters are more important than others in determining the outcome of the system. We used the M-protein level M as the outcome of interest, as M protein continues to be an important measure of tumor burden in patients with MM [20, 24].

We used two sensitivity methods that give different information, as in Olufsen and Ottesen [57] and Marino et al. [50]. Both methods are global, which means that we varied all parameters simultaneously, without fixing any. We varied the parameters by sampling from the parameter space using Latin hypercube sampling (LHS), assuming uniform distributions on each specified parameter range of values. We used global methods because we do not assume any of the parameters have values that are a priori well-estimated or take on fixed values. Identifying sensitive parameters allowed us to subsequently freeze the values of other parameters, and focus on the identifiability and estimation of sensitive parameters.

5.1 Sensitivity Index

For the first method, we computed the sensitivity index which measures the change in the steady-state M value when each parameter is perturbed slightly slightly. Specifically, as in Olufsen and Ottesen [57] and Ingalls [38], we first constructed a sensitivity matrix with (i, j)-th entry corresponding to

$$S_{ij} = \frac{\partial}{\partial p_j}\Big(M(t_i)\Big), \tag{5}$$

where parameter p_j is indexed as in Table 2 ($j = 1,2,...,35$) and time t_i is the discrete time point at which M protein is measured ($i = 1,2,...,K$). We can also express the sensitivity matrix S in the following matrix form,

$$S = \frac{\partial M}{\partial p} = \begin{bmatrix} \frac{\partial M}{\partial p_1}(t_1) & \frac{\partial M}{\partial p_2}(t_1) & \dots & \frac{\partial M}{\partial p_n}(t_1) \\ \frac{\partial M}{\partial p_1}(t_2) & \frac{\partial M}{\partial p_2}(t_2) & \dots & \frac{\partial M}{\partial p_n}(t_2) \\ \vdots & \vdots & \ddots & \vdots \\ \frac{\partial M}{\partial p_1}(t_K) & \frac{\partial M}{\partial p_2}(t_K) & \dots & \frac{\partial M}{\partial p_n}(t_K) \end{bmatrix}. \tag{6}$$

Since different parameters can have different units (and thus can have orders of magnitude difference in size) when compared to M and to each other, we considered the relative sensitivity $\tilde{S}$ by comparing the size of a relative perturbation in parameter p to the resulting relative change in M [38, 57], i.e.,

$$\tilde{S} = \frac{\partial M}{\partial p}\,\frac{p}{M}. \tag{7}$$

Due to the model complexity, we approximated the partial derivatives $\frac{\partial M}{\partial p}$ using a finite difference approximation as in [61, 57],

$$\frac{\partial M}{\partial p_j}(t_i) \approx \frac{M(t_i; p_j + \varepsilon) - M(t_i; p_j)}{\varepsilon},$$

where $\varepsilon \sim \mathscr{O}(\sqrt{10^{-10}})$ and 10^{-10} is the tolerance (size of the absolute error) of the numerical solution of the differential equation. Thus, the sensitivity matrix has an error of $\mathscr{O}(10^{-5})$ [61, 57].

The sensitivity of each parameter p_j is then measured by the *sensitivity index*, defined as the magnitude of the corresponding j-th column of $\tilde{S}$,

$$\bar{S_j} = ||\tilde{S}_j||_2 = \sqrt{\sum_{i=1}^{K}\left(\frac{\partial M}{\partial p_j}(t_i)\frac{p_j}{M(t_i)}\right)^2}. \tag{8}$$

The values of $\bar{S_j}$ can be ordered from largest to smallest, indicating most to least sensitive parameters.

We also considered the subset selection approach presented in [61, 57] when categorizing parameters as sensitive or insensitive. The rank ρ of the relative sensitivity matrix $\tilde{S}$ is computed by finding the number of singular values of $\tilde{S}$ that

are larger than 10^{-5} (since the the sensitivity matrix has an error of $\mathcal{O}(10^{-5})$). The rank ρ defines the number of sensitive parameters. The subset of parameters considered sensitive can be found by considering the following matrix decompositions. Given the singular value decomposition (SVD) of the relative sensitivity matrix, $\tilde{S} = U\Sigma V^T$, we partition V into two blocks, $V = [V_\rho \;\; V_{35-\rho}]$, where V_ρ contains the first ρ columns of V. Then we perform a QR decomposition of V_ρ. That is, we find a permutation matrix P so that $V_\rho^T P = QR$, where Q is an orthogonal matrix and R is an upper triangular matrix whose diagonal elements are arranged in order of decreasing magnitude [33]. The permutation matrix P can then be used to determine the ordering of parameter sensitivity, $\hat{\theta} = P^T\theta$, where $\theta = [1,2,...,35]^T$ and the first ρ entries of $\hat{\theta}$ determines the group of parameters that are considered sensitive.

We performed the local sensitivity analysis outlined above for 10,000 different parameter sets, sampled from the range listed in Table 2 using LHS. For a given parameter set, the relative sensitivity matrix $\tilde{S}$ is computed by simulating the ODE system for 1200 days (with approximate solutions evaluated at $t_i = 0, 30, 60, ..., 1200$ days). We examined both the dependence of long-term/steady-state levels of M protein on the different parameters, and the transition to steady state. For each parameter set, we recorded the sensitivity index of each parameter (Equation (8)) and also kept track of which parameters were identified as sensitive by SVD/QR decomposition.

5.2 Sensitivity of Steady-State Value of M

To examine the sensitivity of the steady-state value of M to changes in each parameter, we recorded the sensitivity index for each parameter (see (8) evaluated for for $t_i \geq 600$ days). Results from 10,000 different parameter sets are shown in Table 3 where the average value of the sensitivity index in Equation (8) for each parameter is listed. The distribution of sensitivity index $\bar{S}_j$ values over the 10,000 parameter sets is shown by parameter in the box plot in Figure 6.

5.3 Sensitivity of Transient Dynamics

We also examined how parameter values may change the time course from initial to steady-state conditions by analyzing the relative sensitivity matrix $\tilde{S}$ evaluated over the full time-course, from 0 to 1200 days. The sensitivity index ordering of parameters listed in Table 3 was preserved. However, subset selection using SVD/QR decompositions gave slightly different results. In Fig. 7, we show the fraction of times (among 10,000 parameter sets) that a particular parameter is characterized as sensitive. The initial value of M, M_0, was characterized as sensitive for all parameter sets. Parameters that govern the dynamics of M in the absence of immune cells, namely δ_M, K_M, r_M, were characterized as next-most sensitive. The top panel

Parameter	$E[\bar{S}_j]$	Parameter	$E[\bar{S}_j]$
δ_M	11.7	a_{CNM}	1.48
δ_N	9.26	s_N	1.09
r_M	9.24	a_{RM}	0.861
δ_C	8.00	a_{MC}	0.775
r_N	7.32	δ_R	0.623
r_C	7.23	r_R	0.618
K_C	4.53	b_{MC}	0.458
a_{NM}	4.49	b_{RM}	0.333
K_N	3.99	K_R	0.332
a_{CM}	3.70	a_{MM}	0.321
a_{CN}	3.41	b_{MM}	0.176
a_{NC}	3.11	a_{MR}	$8.87 \times 10{-}2$
b_{NM}	3.08	b_{MR}	$6.72 \times 10{-}2$
b_{CM}	2.38	M^0	$9.68 \times 10{-}3$
b_{CN}	2.34	T_C^0	$9.39 \times 10{-}3$
b_{NC}	2.06	N^0	$5.52 \times 10{-}3$
K_M	1.74	T_R^0	$8.66 \times 10{-}4$

Table 3 Ordering of parameters from most to least sensitive with respect to steady-state M-protein level, based on average values of the sensitivity index in Equation (8). Results were obtained by averaging over 10,000 sets of parameter values chosen from the range listed in Table 2 using Latin hypercube sampling (LHS).

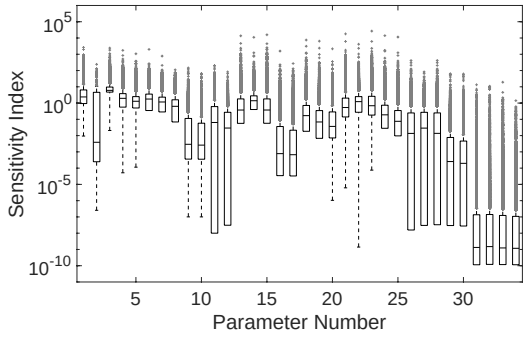

Figure 6 Box plot of sensitivity index value $\bar{S}_j$ for each parameter $j = 1,2,...,35$ (in the order listed in Table 2) for 10,000 parameter sets.

of Fig. 8 shows the fraction of times that the relative sensitivity matrix $\tilde{S}$ has a particular rank; in most trials (87% of 10,000 parameter sets), $\tilde{S}$ has rank between three and eight, indicating that at most eight parameters are considered sensitive. The bottom panel of Fig. 8 shows the distribution of singular values.

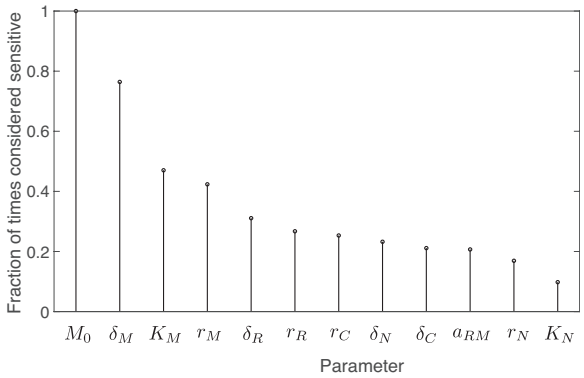

Figure 7 Fraction of times a particular parameter was characterized as sensitive by the SVD/QR subset selection method. Only parameters that were characterized as sensitive at least 10% of times (from 10,000 parameter sets) are shown.

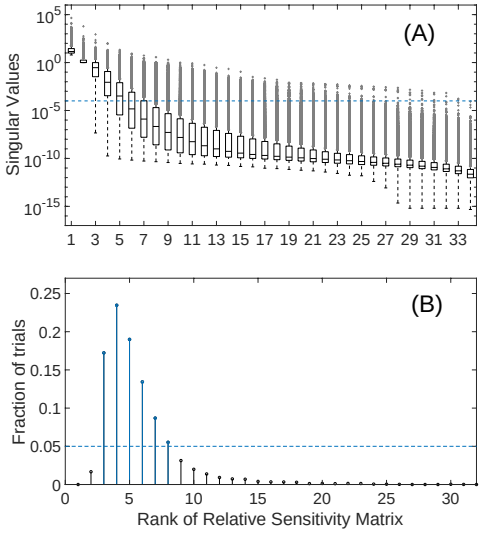

Figure 8 Results from the subset selection approach using SVD/QR decomposition. *(A):* Box plot of singular values of $\tilde{S}$ (blue dashed line shows the threshold value of 10^{-4} for computing the matrix rank), *(B):* Histogram of Rank($\tilde{S}$) (blue dashed line shows the threshold for 5% of all trials).

5.4 Sensitivity from PRCC

The second sensitivity method we used was partial rank correlation coefficients (PRCC), as discussed in [50]. We used LHS to uniformly sample the parameter space and then uses PRCC to determine the monotonicity of the relationships between the parameters and the system output. A PRCC value of 1 indicates a strictly increasing relationship, while a PRCC value of -1 indicates a strictly decreasing relationship.

We sampled 10,000 parameter sets from the ranges in Table 2 using LHS. For each parameter set, we computed the steady-state solution by simulating the system of Equations (1)-(4) until the solution $\mathbf{y} = (M, T_C, N, T_R)$ satisfied $\frac{\|\mathbf{y}(t_{i+1}) - \mathbf{y}(t_i)\|}{\|\mathbf{y}(t_i)\|} < 10^{-8}$. We evaluated sensitivities using PRCC on the same 10,000 sets of parameter values, computed in Matlab.

Sensitivity coefficients and the corresponding p-values for each parameter are listed in Table 4 and displayed graphically in Figure 9. The sensitivity analysis shows that there are 24 parameters that have a statistically significant PRCC value, assuming a p-value cutoff of 0.01. There are 10 parameters that have statistically insignificant PRCC values, including all four initial conditions.

The system is most sensitive to the basal death and replication rates of M (δ_M and r_M, respectively). The system is also highly sensitive to the replication and death rates of cytotoxic T cells and NK cells (r_C, δ_C, r_N, and δ_N) and the effects of NK and T cells on M. Scatter plots of the steady-state M values vs. the eight most sensitive parameters are shown in Figure 10. The system appears to be insensitive to the Treg dynamics and all four initial conditions.

Parameter	PRCC	p-value	Parameter	PRCC	p-value
δ_M	-0.77506	0	b_{CN}	0.071022	1.2607e-12
r_M	0.50157	0	a_{RM}	0.063225	2.6573e-10
r_C	-0.43832	0	δ_R	-0.057886	7.3297e-09
r_N	-0.35586	0	s_N	-0.05191	2.1566e-07
a_{NM}	-0.35159	0	b_{RM}	-0.048376	1.3529e-06
a_{CM}	-0.33998	0	a_{MC}	-0.047831	1.7762e-06
δ_N	0.32594	0	r_R	0.033966	0.00069492
δ_C	0.32128	0	b_{MM}	-0.019666	0.049612
b_{NM}	0.28765	0	K_R	0.01798	0.072653
b_{CM}	0.2628	0	N^0	-0.014379	0.15117
a_{NC}	-0.19504	0	M^0	0.01266	0.20631
a_{CNM}	-0.17783	0	a_{MM}	0.010565	0.29157
a_{CN}	-0.17034	0	b_{MC}	0.010241	0.30664
K_C	-0.11739	0	b_{MR}	0.0091194	0.36264
b_{NC}	0.086461	0	T_R^0	0.0053638	0.59235
K_M	0.08043	0	a_{MR}	0.0038526	0.70056
K_N	-0.07497	6.6707e-14	T_C^0	-0.003647	0.71582

Table 4 Table of PRCC values by parameter, in order of descending magnitude, and their corresponding p-values (p-values smaller than 10^{-14} are rounded to 0). The response variable is the steady-state value of M. Results were obtained using LHS/PRCC with 10,000 samples.

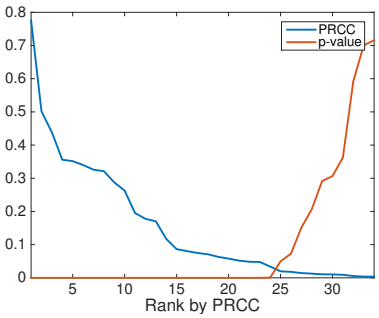

Figure 9 Plot of PRCC and p-values for 34 parameters (s_M fixed), ranked from highest to lowest PRCC.

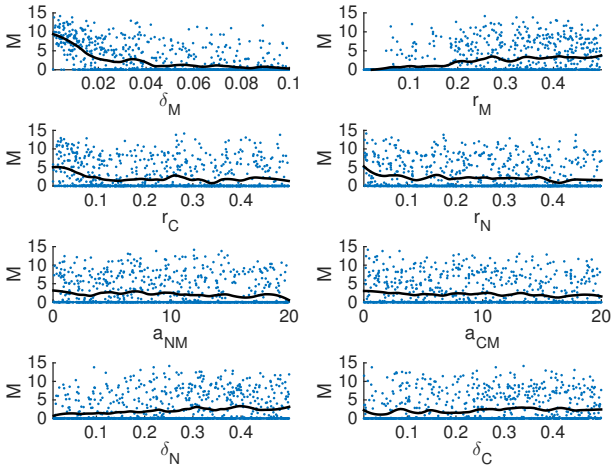

Figure 10 Scatter plots of steady-state M values vs. the eight most sensitive parameters, with 1000 samples. Black curves indicate a loess fit to the data.

5.5 Comparisons between Sensitivity Index and PRCC Methods

We next compared the results obtained from the two methods of measuring parameter sensitivity as summarized in Tables 3-4. Looking at the 10 most sensitive parameters measured by each method (first ten listed on each Table), we observed that there are eight parameters shared in common, namely $\delta_M, r_M, \delta_N, r_N, \delta_C, r_C, a_{NM}, a_{CM}$.

From here on, we considered the effects of varying these eight parameters while holding the rest fixed at the values listed on the Used Column in Table 2.

5.6 Sensitivity: Graphical Exploration

Here, we show numerical simulations that highlight how slight variations in sensitive parameters can shift the model outcome between one of the two steady-states illustrated in our bistability simulations (those shown in Figure 4).

As described above in Section 5, our sensitivity analysis measures sensitivity by looking at how the M-protein level, $M(t)$, varies according to small changes in parameter values. Results of this analysis indicate that two of the most sensitive parameters are the decay rate for M, δ_M, and the proliferation rate for M, r_M (see Tables 3 and 4).

In Figures 11 and 12, we show the effect of varying δ_M and r_M on final M steady-state values. The solid black curves correspond to the steady-state values illustrated in Figure 4. In particular, each solid black curves to the left correspond to high steady-state values of M (attained for initial condition $M(0) = 1.92$), and those to the right correspond to low steady-state values of M (attained for initial condition $M(0) = 0.96$). The dashed black curves indicate the change/switch in steady-state behavior, due to a small variation in the indicated parameter. In each of Figures 11 and 12, we note that small variations in the indicated parameter results in a change in the long-term dynamics of the M population.

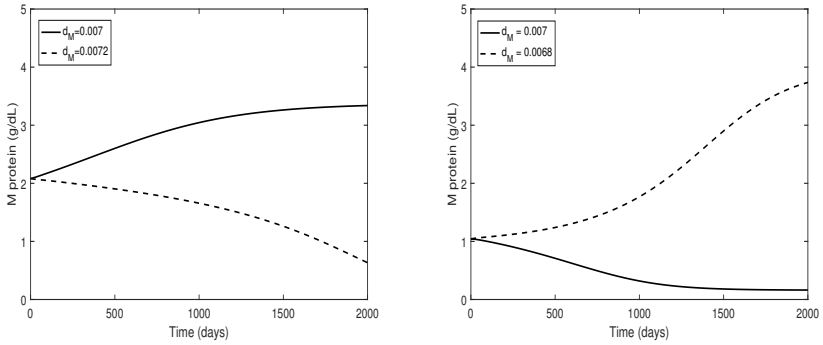

Figure 11 Effect of varying δ_M on final M values. Here, the solid black curves correspond to the M concentrations illustrated in Figure 4, while the dotted black curves correspond to the change in M due to a change in the indicated parameter. **(left):** Switch from state of high tumor burden to LTDC for increasing δ_M. **(right):** Switch from state of LTDC to a state of high tumor burden for decreasing δ_M. All parameters are the same as those used in Figure 4.

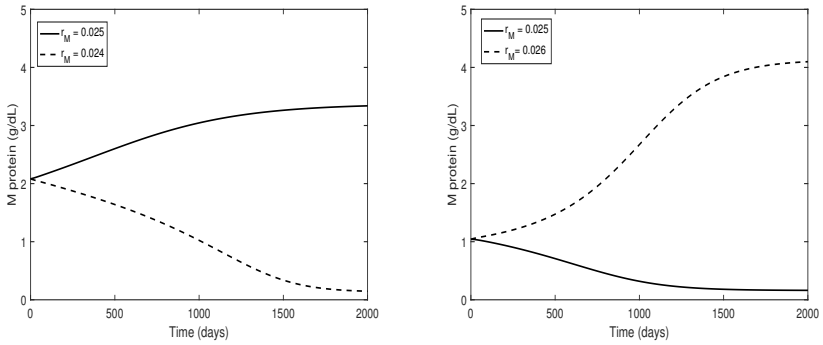

Figure 12 Effect of varying r_M on final M values. Here, the solid black curves correspond to the M concentrations illustrated in Figure 4, while the dotted black curves correspond to the change in M due to a change in the indicated parameter. **(left):** Switch from state of high tumor burden to LTDC for decreasing r_M. **(right):** Switch from state of LTDC to a state of high tumor burden for increasing r_M. All parameters are the same as those used in Figure 4.

6 Identifiability

With a more clear view of the sensitive parameters for our model, we now examine the structural non-identifiability of the model. The primary item of interest here is whether it is possible to uniquely determine a set of sensitive parameters in the ideal scenario of continuous error-free data for the four relevant model populations, M, T_C, N, T_R. Model non-identifiability could be thought to arise when the model is over-parametrized; a priori global identifiability is thus a structural property of the model, and must be considered a prerequisite step for parameter estimation. The question that one can ask in this context is this: given two sets of arbitrary parameter values and assuming that the model is initialized at the same initial state, does there exist at least an input function for which the model with the two parameter sets yields different outputs?

There are three possible outcomes for the identifiability for a model:

- Globally or uniquely identifiable from data. In this case two distinct sets of parameter values can be distinguished from input-output data.
- Non-identifiable. In this case two distinct parameter sets yield the same output no matter what input function is applied and no matter the initial conditions.
- Locally (or non-uniquely) identifiable. There are at most a finite number of indistinguishable parameter values.

There are multiple approaches for determining model identifiability. We performed identifiability analysis of the model using the MATLAB package GenSSI ([11]), which handles nonlinear systems of differential equations by applying a power series approach. Briefly, GenSSI uses Lie derivatives of the model system in order to construct a system of equations; in turn the solvability properties of these equations

are used to provide information about the global and local structural identifiability as well as non-identifiability. A nice feature of the GenSSI approach is that besides providing a text result that presents the solutions to algebraic relations, it also provides a graphical representation through the generation of *identifiability tableaus* [11]. The identifiability tableaus are binary representations of the Jacobian of the series coefficients with respect to the parameters with as many columns as parameters and with as many rows as non-zero series coefficients [3]. Values of one are shown as black, and values of zero are shown as white. Since the number of series coefficients may be infinite in principle, non-identifiability is not guaranteed for an arbitrary model [3]. The rank of the Jacobian is used by GenSSI to establish solvability properties. The structure of the tableaus is used to help decide how to solve equations for a particular parameter. Specifically, the GenSSI Jacobian matrix rank obtained by taking a predefined set of derivatives must match the number of unknown model parameters in order for local identifiability to be guaranteed. For the generated tableaus, columns consisting solely of zeros indicate that the respective parameter cannot be identified and rows consisting solely of zeros provide no information and are deleted in successive tableau reducing steps. Tableau rows that consist of two or more ones indicate that there are relations that must be solved algebraically to provide identifiability. Solving these remaining algebraic relations is where the algorithm spends most of the time.

6.1 Identifiability of the model, allowing the eight most-sensitive parameters to vary

In this section, we study the model by setting all parameters to the Used column values in Table 2, except for the top eight most-sensitive ones as obtained in the previous section. These eight parameters are considered unknown in the model and we explore whether they could be identified with error-free time series data. The eight parameters allowed to vary here are $r_M, \delta_M, r_C, \delta_C, r_N, \delta_N, a_{NM}$, and a_{CM}. We assume that we have information on all four populations in our model, meaning we have error-free time series data on M, T_C, N, T_R, including the initial conditions (as listed in Table 2).

The result from GenSSi for this case is that the eight most-sensitive parameters for our model are **globally structurally identifiable** which indicates that error-free time series data tracking the four relevant model populations are sufficient to identify a unique parameter set from the eight most-sensitive parameter list. The reduced identifiability tableau is shown in Fig. 13.

If more parameters are added to the free parameter list (for example, carrying capacity parameters, which rank high in sensitivity), then we get locally identifiable results. This indicates that the top eight most-sensitive parameters in our model are a priori identifiable. Next, we pursue practical (or a posteriori) identifiability. That is, we test whether it is possible to evaluate parameters from a given set of experimental data subject to experimental noise, explored in the next section.

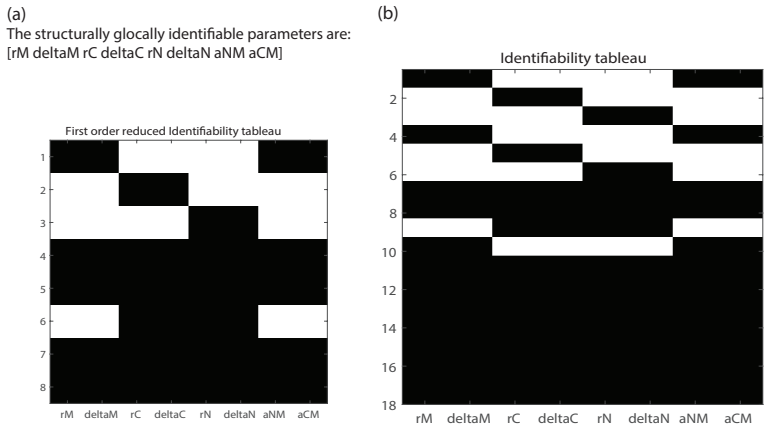

Figure 13 Model identifiability results with eight most-sensitive parameters allowed to vary. Black blocks represent values of one; white blocks represent values of zero. (a) Results and reduced tableau (b) Identifiability tableau. All eight parameters are globally identifiable.

6.2 Practical identifiability – MCMC

The above structural identifiability results assume the availability of noiseless, complete time-series data. In practice, such data are not available; thus it is worth exploring whether the eight most-sensitive parameters are identifiable from, for example, noisy steady-state data. If we assume that patients are at a steady state at the time of diagnosis, we may use clinical data to try to infer parameter values. Pessoa et al. [59] provide means and standard deviations for the three cell populations (T_C, N, T_R) for patients with MM. The mean and standard deviation of M protein from patients prior to treatment were obtained from [35, 79].

We make the additional assumption that the cell populations are log-normally distributed, and seek to identify parameter distributions given the assumed parameter ranges (Table 2) and the distributions of the data. It should be noted that the published data show large variances. In particular, the standard deviation of the T_C population size is almost as large as the mean.

To estimate the parameter distributions, we used a Markov chain Monte Carlo (MCMC) method. The Markov chain consisted of 100,000 samples obtained via Metropolis-Hastings sampling. Prior distributions for the parameters were taken to be uniform within the ranges in Table 2, with the growth and death rates (r_i and δ_i, respectively) taken on a log scale. The resulting parameter distributions are presented in Figure 14 in the form of one-dimensional histograms and two-dimensional heat maps.

We see that many of the parameters have broad distributions and thus are not practically identifiable given the available steady-state data. This is not surprising given the large amount of uncertainty in the data itself. However, it is clear from

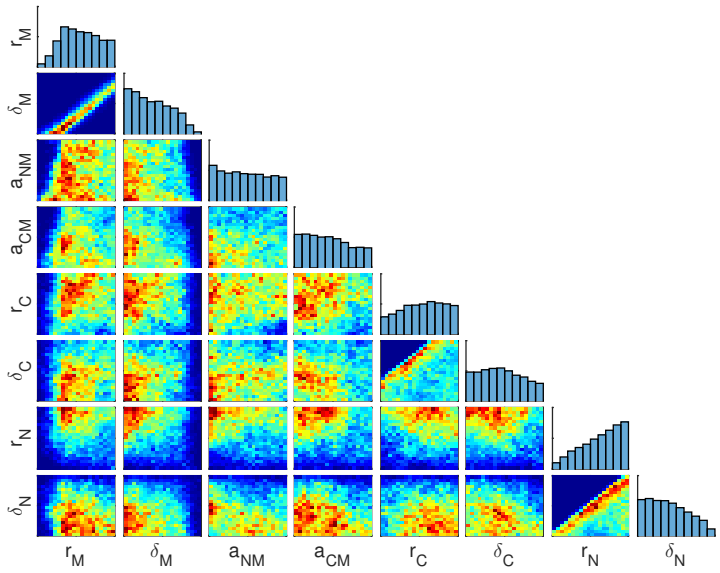

Figure 14 Matrix of two-dimensional heat maps showing the parameter distribution obtained via MCMC, with one-dimensional histograms on the diagonal. In the heat maps, red indicates an area of high density and blue indicates an area of low density. The axis limits are given by the parameter ranges in Table 2. Axes for r and δ parameters are on a log scale.

Figure 14 that $\log(r_M)$ and $\log(\delta_M)$ have a strong linear relationship with slope approximately one. Thus, while the parameters themselves are not identifiable, a linear combination of them is. Similar (but weaker) relationships are apparent between r_C and δ_C and between r_N and δ_N.

Figure 15 shows the distributions for the four populations M, T_C, N, and T_R for the MCMC chain. While the M distribution matches the assumed distribution well, the immune cell populations do not match the data well. In particular, the T_C and N compartments tend toward their respective carrying capacities and cluster there, while the T_R compartment size is tightly controlled. This may indicate that we are neglecting the parameters responsible for controlling these cell populations. For example, since the replication/death rates and carrying capacity of T_R are fixed, we would expect its steady-state population size to have small variance. This is in agreement with the Pessoa et al. [59] data, in which the Treg populations are similar among healthy volunteers and patients with various stages of MM.

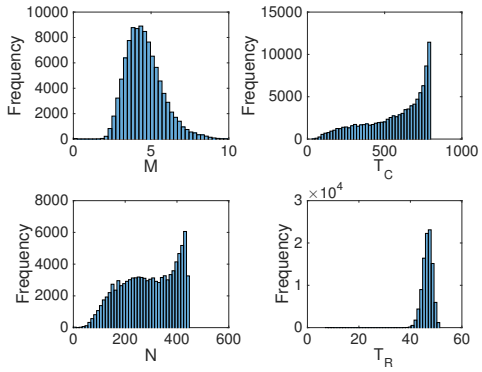

Figure 15 Distributions of the four populations M, T_C, N, and T_R for the MCMC chain.

7 Conclusion

We have explored a mathematical model that was originally presented in [29]. This model uses immune cell and M-protein populations in the peripheral blood to represent the dynamics of disease burden and immune response in a patient with MM. The value of a model depends not only on the model structure, but also on the parameter values used with the model. In Gallaher et al. [29], our focus was on the model structure; in this work, we focused on the parameter values and ranges. We provided detailed information on parameter estimates based on studies in the literature and justified any necessary calculations. We performed global sensitivity analyses to identify key parameters that affect the model dynamics. We considered the identifiability of the entire system, as well as subsets of sensitive parameters, to determine when the parameters can be estimated from clinical data. We used available summary steady-state data in the literature from patients with MM to inform parameter values. And we looked at multiple numerical solutions of the system, with the sensitive parameters varied through a range of values.

When we compared outcomes from two different global sensitivity methods, we found that the top ten sensitive parameters of each method (results shown in Tables 3 and 4) have eight parameters in common. The SVD/QR decomposition results support up to eight sensitive parameters. Our core of eight most-sensitive parameters is comprised of δ_M, δ_N, r_M, δ_C, r_N, r_C, a_{NM}, and a_{CM}. Note that none of the parameters directly related to the size of the Treg population appeared among the top most-sensitive parameters. This appears to be in agreement with the data in Pessoa et al. [59] showing that there are not significant differences in Treg levels between healthy adults and patients with various stages of MM.

We allowed the set of eight most-sensitive parameters to vary in explorations of the model, while we fixed the values of the other parameters. Small changes in the sensitive parameters can result in large changes in the steady-state value of M. The

sensitive parameters thus may indicate vulnerabilities in the model pathways for therapeutic intervention, which can indicate promising therapies to try in combination.

The behavior of the model system for different values of two of the most sensitive parameters, δ_M and r_M, can be seen in Figs. (11)-(12). The widely different outcomes when these sensitive parameters are varied agree with the bistable behavior found previously in the analysis in Gallaher et al. [29].

Limitations of our model include the following: 1) our model tracks populations in the peripheral blood, though MM is a disease based in the bone marrow; and 2) our model includes terms in Equation (1) that represent immune system removal of M protein even in the absence of disease, which may not be accurate. Additionally, our ability to estimate parameters for this model would be improved if time series data were available from individual patients with MM who have not yet been treated, perhaps from historical data sets.

The careful parameter estimation, the work to determine sensitive parameters in the model, the identifiability analysis, re-examination of parameter values for the sensitive parameters, and the numerical simulations, all add confidence to the structure and the parameter values of the model. This work provides the necessary foundation for a natural next step: the prediction of optimal combination regimens for patients with MM, and the experimental validation of such a prediction.

Acknowledgements This work was initiated during the Association for Women in Mathematics collaborative workshop Women Advancing Mathematical Biology hosted by the Mathematical Biosciences Institute (MBI) at Ohio State University in April 2017. Funding for the workshop was provided by MBI, NSF ADVANCE "Career Advancement for Women Through Research-Focused Networks" (NSF-HRD 1500481), Society for Mathematical Biology, and Microsoft Research.

References

1. Abdul K Abbas, Andrew H Lichtman, and Shiv Pillai. *Cellular and Molecular Immunology, Eighth Edition*. Elsevier Saunders, Philadelphia, PA, 2015.
2. JC Arciero, TL Jackson, and DE Kirschner. A mathematical model of tumor-immune evasion and siRNA treatment. *Discrete and Continuous Dynamical Systems Series B*, 4(1):39–58, 2004.
3. Eva Balsa-canto, Antonio A Alonso, and Julio Banga. An iterative identification procedure for dynamic modeling of biochemical networks. *BMC Systems Biology*, 4:11.
4. Rob J De Boer, Pauline Hogeweg, Hub FJ Dullens, Roel A De Weger, and Willem Den Otter. Macrophage T lymphocyte interactions in the anti-tumor immune response: a mathematical model. *The Journal of Immunology*, 134(4):2748–2758, 1985.
5. Rob J De Boer, Dirk Homann, and Alan S Perelson. Different dynamics of CD4+ and CD8+ T cell responses during and after acute lymphocytic choriomeningitis virus infection. *The Journal of Immunology*, 171(8):3928–3935, 2003.
6. Onur Boyman and Jonathan Sprent. The role of interleukin-2 during homeostasis and activation of the immune system. *Nature Reviews Immunology*, 12(3):180, 2012.
7. RD Brown, B Pope, E Yuen, J Bibson, and DE Joshua. The expression of T cell related costimulatory molecules in multiple myeloma. *Leukemia & Lymphoma*, 31(3-4):379–384, 1998.

8. Ennio Carbone, Paola Neri, Maria Mesuraca, Mariateresa T Fulciniti, Takemi Otsuki, Daniela Pende, Veronika Groh, Thomas Spies, Giuditta Pollio, David Cosman, Lucio Catalano, Pierfrancesco Tassone, Bruno Rotoli, and Salvatore Venuta. HLA class I, NKG2D, and natural cytotoxicity receptors regulate multiple myeloma cell recognition by natural killer cells. *Immunobiology*, 105(1):251–258, 2005.
9. Adelheid Cerwenka, Jody Baron, and Lewis Lanier. Ectopic expression of retinoic acid early inducible-1 gene (RAE-1) permits natural killer cell-mediated rejection of a MHC class I-bearing tumor in vivo. *Proceedings of the National Academy of Sciences*, 98(20):11521–11526, 2001.
10. Mei-Ling Chen, Mikaël J Pittet, Leonid Gorelik, Richard A Flavell, Ralph Weissleder, Harald von Boehme, and Khashayarsha Khazaie. Regulatory T cells suppress tumor-specific CD8 T cell cytotoxicity through TGF-β signals in vivo. *Proceedings of the National Academy of Sciences*, 102(2):419–424, 2005.
11. Oana Chiş, Julio R. Banga, and Eva Balsa-Canto. GenSSI: a software toolbox for structural identifiability analysis of biological models. *Bioinformatics*, 27:2610–2611, 2011.
12. Andrea K Cooper and Peter S Kim. A cellular automata and a partial differential equation model of tumor-immune dynamics and chemotaxis. In Amina Eladaddi, Peter Kim, and Dann Mallet, editors, *Mathematical Models of Tumor-Immune System Dynamics*, volume 107 of *Springer Proceedings in Mathematics and Statistics*, pages 21–46. Springer, New York, 2014.
13. Giovanni D'Arena, Giovanni Rossi, Luca Laurenti, Teodora Statuto, Fiorella D'Auria, Luciana Valvano, Vittorio Simeon, Aldo Giudice, Idanna Innocenti, Vincenzo De Feo, Rosanna Filosa, and Pellegrino Musto. Circulating regulatory T-cells in monoclonal gammopathies of uncertain significance and multiple myeloma: In search of a role. *Journal of Immunology Research*, 2016:Article ID 9271469, 2016.
14. Lisette de Pillis, Trevor Caldwell, Elizabeth Sarapata, and Heather Williams. Mathematical modeling of regulatory T cell effects on renal cell carcinoma treatment. *Discrete & Continuous Dynamical Systems-Series B*, 18(4), 2013.
15. Lisette G de Pillis, Ami Radunskaya, and Charles L Wiseman. A validated mathematical model of cell-mediated immune response to tumor growth. *Cancer Research*, 65:7950–7958, 2005.
16. Harold P de Vladar and Jorge A González. Dynamic response of cancer under the influence of immunological activity and therapy. *Journal of Theoretical Biology*, 227(3):335–348, 2004.
17. Marcello Delitalia, Tommaso Lorenzi, and Matteo Melensi. A structured population model of competition between cancer cells and T cells under immunotherapy. In Amina Eladaddi, Peter Kim, and Dann Mallet, editors, *Mathematical Models of Tumor-Immune System Dynamics*, volume 107 of *Springer Proceedings in Mathematics and Statistics*, pages 47–58. Springer, New York, 2014.
18. Madhav V Dhodapkar, Matthew D Geller, David H Chang, Kanako Shimizu, Shin-Ichiro Fujii, Kavita M Dhodapkar, and Joseph Krasovsky. A reversible defect in natural killer T cell function characterizes the progression of premalignant to malignant multiple myeloma. *Journal of Experimental Medicine*, 197(12):1667–1676, 2003.
19. Andreas Diefenbach, Eric R Jensen, Amanda M Jamieson, and David H Raulet. Rae1 and H60 ligands of the NKG2D receptor stimulate tumor immunity. *Nature*, 413(6852):165, 2001.
20. Meletios Dimopoulos, Robert Kyle, Jean-Paul Fermand, S Vincent Rajkumar, Jesus San Miguel, Asher Chanan-Khan, Heinz Ludwig, Douglas Joshua, Jayesh Mehta, Morie Gertz, Hervé Avet-Loiseau, Meral Beksaç, Kenneth C Anderson, Philippe Moreau, Seema Singhal, Hartmut Goldschmidt, Mario Boccadoro, Shaji Kumar, Sergio Giralt, Nikhil C. Munshi, and Sundar Jagannath, on behalf of the International Myeloma Workshop Consensus Panel 3. Consensus recommendations for standard investigative workup: report of the International Myeloma Workshop Consensus Panel 3. *Blood*, 117(18):4701–4705, 2011.
21. Richard J DiPaolo, Deborah D Glass, Karen E Bijwaard, and Ethan M Shevach. CD4+ CD25+ T cells prevent the development of organ-specific autoimmune disease by inhibiting the differentiation of autoreactive effector T cells. *Journal of Immunology*, 175(11):7135–7142, 2005.

22. Alberto d'Onofrio. A general framework for modelling tumor-immune system competition and immunotherapy: Mathematical analysis and biomedical inferences. *Physica D*, 208(3-4):202–235, 2005.
23. T Dosani, M Carlsten, I Maric, and O Landgren. The cellular immune system in myelomagenesis: NK cells and T cells in the development of MM and their uses in immunotherapies. *Blood Cancer Journal*, 5(4):e306, 2015.
24. Brian GM Durie and Sydney E Salmon. A clinical staging system for multiple myeloma: Correlation of measured myeloma cell mass with presenting clinical features, response to treatment, and survival. *Cancer*, 36:842–854, 1975.
25. James Favaloro, Ross Brown, Esther Aklilu, Shihong Yang, Hayley Suen, Derek Hart, Phillip Fromm, John Gibson, Liane Khoo, P Joy Ho, and Douglas Joshua. Myeloma skews regulatory T and pro-inflammatory T helper 17 cell balance in favor of a suppressive state. *Leukemia & Lymphoma*, 55(5):10901098, 2014.
26. Sylvia Feyler, Gina B Scott, Christopher Parrish, Sarah Jarmin, Paul Evans, Mike Short, Katherine McKinley, Peter J Selby, and Gordon Cook. Tumour cell generation of inducible regulatory T-cells in multiple myeloma is contact-dependent and antigen-presenting cell-independent. *PLOS ONE*, 7(5):e35981, 2012.
27. Sylvia Feyler, Marie von Lilienfeld-Toal, Sarah Jarmin, Lee Marles, Andy Rawstron, AJ Ashcroft, Roger G Owen, Peter J Selby, and Gordon Cook. CD4+CD25+FoxP3+ regulatory T cells are increased whilst CD3+CD4CD8abTCR+ double negative T cells are decreased in the peripheral blood of patients with multiple myeloma which correlates with disease burden. *British Journal of Haematology*, 144:686695, 2009.
28. Christoph Frohn, Maike Hoppner, Peter Schlenke, Holger Kirchner, Petra Koritke, and Jurgen Luhm. Anti-myeloma activity of natural killer lymphocytes. *British Journal of Haematology*, 119:660–664, 2002.
29. Jill Gallaher, Kamila Larripa, Urszula Ledzewicz, Marissa Renardy, Blerta Shtylla, Nessy Tania, Diana White, Karen Wood, Li Zhu, Chaitali Passey, Michael Robbins, Natalie Bezman, Suresh Shelat, Hearn Jay Cho, and Helen Moore. A mathematical model for tumor-immune dynamics in multiple myeloma. *Submitted*, 2017.
30. Minjie Gao, Lu Gao, Guang Yang, Yi Tao, Jun Hou, Hongwei Xu, Xiaojing Hu, Ying Han, Qianqiao Zhang, Fenghuang Zhan, Xiaosong Wu, and Jumei Shi. Myeloma cells resistance to NK cell lysis mainly involves an HLA class I-dependent mechanism. *Acta Biochimica et Biophysica Sinica*, 46(7):597–604, 2014.
31. François Ghiringhelli, Cédric Ménard, Francois Martin, and Laurence Zitvogel. The role of regulatory T cells in the control of natural killer cells: Relevance during tumor progression. *Immunological Reviews*, 214(1):229–238, 2006.
32. François Ghiringhelli, Cédric Ménard, Magali Terme, Caroline Flament, Julien Taieb, Nathalie Chaput, Pierre E Puig, Sophie Novault, Bernard Escudier, Eric Vivier, et al. CD4+ CD25+ regulatory T cells inhibit natural killer cell functions in a transforming growth factor-β-dependent manner. *Journal of Experimental Medicine*, 202(8):1075–1085, 2005.
33. Gene H Golub and Charles F Van Loan. *Matrix computations*, volume 3. Johns Hopkins Studies in Mathematical Sciences, 2012.
34. A. Gonzalez-Qunitela, R. Alende, F. Gude, J. Campos, J. Rey, and L.M. Meijide. Serum levels of immunoglobulins (igg, iga, igm) in a general adult population and their relationship with alcohol consumption, smoking and common metabolic abnormalities. *Clinical & Experimental Immunology*, 151(5):42–50, 2008.
35. Philip R Greipp, Jesus San Miguel, Brian GM Durie, John J Crowley, Bart Barlogie, Joan Bladé, Mario Boccadoro, J Anthony Child, Hervé Avet-Loiseau, Robert A Kyle, Juan J Lahuerta, Heinz Ludwig, Gareth Morgan, Raymond Powles, Kazuyuki Shimizu, Chaim Shustik, Pieter Sonneveld, Patrizia Tosi, Ingemar Turesson, and Jan Westin. International staging system for multiple myeloma. *Journal of Clinical Oncology*, 23(15):3412–3420, 2005.
36. Charlotte T Hansen, Per T Pedersen, Lars C Nielsen, and Niels Abildgaard. Evaluation of the serum free light chain (sFLC) analysis in prediction of response in symptomatic multiple myeloma patients: Rapid profound reduction in involved FLC predicts achievement of VGPR. *European Journal of Haematology*, 93(5):407–413, 2014.

37. James A Hokanson, Barry W Brown, James R Thompson, Benjamin Drewinko, and Raymond Alexanian. Tumor growth patterns in multiple myeloma. *Cancer*, 39:1077–1084, 1977.
38. Brian P Ingalls. *Mathematical modeling in systems biology: an introduction*. MIT Press, 2013.
39. Charles A Janeway. How the immune system protects the host from infection. *Microbes and Infection*, 3(13):1167–1171, 2001.
40. F Jonsson, Y Ou, L Claret, D Siegel, S Jagannath, R Vij, A Badros, S Aggarwal, and R Bruno. A tumor growth inhibition model based on M-protein levels in subjects with relapsed/refractory multiple myeloma following single-agent carfilzomib use. *CPT: Pharmacometrics & Systems Pharmacology*, 4(12):711–719, 2015.
41. You Kawarada, Ruth Ganss, Natalio Garbi, Torsten Sacher, Bernd Arnold, and Günter J Hämmerling. NK- and CD8+ T cell-mediated eradication of established tumors by peritumoral injection of CpG-containing oligodeoxynucleotides. *The Journal of Immunology*, 167(9):5247–5253, 2001.
42. Dickran Kazandjian and Ola Landgren. A look backward and forward in the regulatory and treatment history of multiple myeloma: Approval of novel-novel agents, new drug development, and longer patient survival. *Seminars in Oncology*, 43:682689, 2016.
43. Jeong M Kim, Jeffrey P Rasmussen, and Alexander Y Rudensky. Regulatory T cells prevent catastrophic autoimmunity throughout the lifespan of mice. *Nature Immunology*, 8(2):191, 2007.
44. Denise Kirschner and John Carl Panetta. Modeling immunotherapy of the tumor-immune interaction. *Journal of Mathematical Biology*, 37:235–252, 2007.
45. Shaji Kumar, S Vincent Rajkumar, Philip R Greipp, and Thomas E Witzig. Cell proliferation of myeloma plasma cells: Comparison of the blood and marrow compartments. *Pharmaceuticals (Basel)*, 77:7–11, 2004.
46. Vladimir A Kuznetsov, Iliya A Makalkin, Mark A Taylor, and Alan S Perelson. Nonlinear dynamics of immunogenic tumors: Parameter estimation and global bifurcation analysis. *Bulletin of Mathematical Biology*, 56(2):295–321, 1994.
47. Robert A Kyle, Morie A Gertz, Thomas E Witzig, John A Lust, Martha Q Lacy, Angela Dispenzieri, Rafael Fonseca, S Vincent Rajkumar, Janice R Offord, Dirk R Larson, et al. Review of 1027 patients with newly diagnosed multiple myeloma. In *Mayo Clinic Proceedings*, volume 78, pages 21–33. Elsevier, 2003.
48. Christof Lehman, Matthias Zeis, and Lutz Uharek. Activation of natural killer cells with interleukin 2 (IL-2) and IL-12 increases perforin binding and subsequent lysis of tumour cells. *British Journal of Haematology*, 114(3):660–665, 2001.
49. Kang-Ling Liao, Xue-Feng Bai, and Avner Friedman. Mathematical modeling of interleukin-27 induction of anti-tumor T cells response. *PLOS ONE*, 9(3):e91844, 2014.
50. Simeone Marino, Ian B Hogue, Christian J Ray, and Denise E Kirschner. A methodology for performing global uncertainty and sensitivity analysis in systems biology. *Journal of Theoretical Biology*, 254:178–196, 2008.
51. Thorsten R Mempel, Mikael J Pittet, Khashayarsha Khazaie, Wolfgang Weninger, Ralph Weissleder, Harald von Boehmer, and Ulrich H von Andrian. Regulatory T cells reversibly suppress cytotoxic T cell function independent of effector differentiation. *Immunity*, 25(1):129–141, 2006.
52. Neal J Meropol, Grace M Barresi, Todd A Fehniger, James Hitt, Margaret Franklin, and Michael A Caligiuri. Evaluation of natural killer cell expansion and activation in vivo with daily subcutaneous low-dose interleukin-2 plus periodic intermediate-dose pulsing. *Cancer Immunology and Immunotherapy*, 46(6):318–326, 1998.
53. JR Mills, DR Barnidge, A Dispenzieri, and DL Murray. High sensitivity blood-based M-protein detection in sCR patients with multiple myeloma. *Blood Cancer Journal*, 7(8):e590, 2017.
54. Helen Moore and Natasha K Li. A mathematical model for chronic myelogenous leukemia (CML) and T cell interaction. *Journal of Theoretical Biology*, 227(4):513–523, 2004.
55. Charvi Nanavati, Donna Ruszaj, and Donald E. Mager. Cell signaling model connects vorinostat pharmacokinetics and tumor growth response in multiple myeloma xenografts. *CPT Pharmacometrics Syst. Pharmacol.*, 6:756–764, 2017.

56. Tricia Nardiello, Achim A Jungbluth, Anna Mei, Maurizio DiLiberto, Xiangao Huang, Valeria CC Andrade Ania Dabrowski, Rebecca Wasserstrum, Scott Ely, Ruben Niesvizky, Roger Pearse, Morton Coleman, David S Jayabalan, Nina Bhardwaj, Lloyd J Old, Selina Chen-Kiang, and Hearn Jay Cho. MAGE-A inhibits apoptosis in proliferating myeloma cells through repression of Bax and maintenance of survivin. *Clinical Cancer Research*, 17(13):4309–4319, 2011.
57. Mette S Olufsen and Johnny T Ottesen. A practical approach to parameter estimation applied to model predicting heart rate regulation. *Journal of Mathematical Biology*, 67(1):39–68, 2013.
58. Katharina Pallmer and Annette Oxenius. Recognition and regulation of T cells by NK cells. *Frontiers in Immunology*, 7, 2016.
59. Roberto J Pessoa de Magalhães, María-Belén Vidriales, Bruno Paiva, Carlos Fernandez-Gimenez, Ramón García-Sanz, Maria-Victoria Mateos, Norma C Gutierrez, Quentin Lecrevisse, Juan F Blanco, Jose Hernández, Natalia de las Heras, Joaquin Martinez-Lopez, Monica Roig, Elaine Sobral Costa, Enrique M Ocio, Martin Perez-Andres, Angelo Maiolino, Marcio Nucci, Javier De La Rubia, Juan-Jose Lahuerta, Jesús F San-Miguel, and Alberto Orfao. Analysis of the immune system of multiple myeloma patients achieving long-term disease control by multidimensional flow cytometry. *Haematologica*, 98(1):79–86, 2013.
60. A Plebani, AG Ugazio, MA Avanzini, P Massimi, L Zonta, V Monafo, and GR Burgio. Serum IgG subclass concentrations in healthy subjects at different age: age normal percentile charts. *European Journal of Pediatrics*, 149(3):164–167, 1989.
61. Scott R Pope, Laura M Ellwein, Cheryl L Zapata, Vera Novak, C Tim Kelley, and Mette S Olufsen. Estimation and identification of parameters in a lumped cerebrovascular model. *Math Biosci Eng*, 6(1):93–115, 2009.
62. Guy Pratt, Oliver Goodyear, and Paul Moss. Immunodeficiency and immunotherapy in multiple myeloma. *British Journal of Haematology*, 138:563–579, 2007.
63. M Raitakari, RD Brown, J Gibson, and DE Joshua. T cells in myeloma. *Hematological Oncology*, 21(1):33–42, 2003.
64. Karthick Raja Muthu Raja, Lucie Rihova, Lenka Zahradova, Maria Klincova, Miroslav Penka, and Roman Hajek. Increased T regulatory cells are associated with adverse clinical features and predict progression in multiple myeloma. *PLOS ONE*, 7(10):e47077, 2012.
65. Mark Robertson-Tessi, Ardith El-Kareh, and Alain Goriely. A mathematical model of tumor-immune interactions. *Journal of Theoretical Biology*, 294:56–73, 2012.
66. Sydney E Salmon and Beth A Smith. Immunoglobulin synthesis and total body tumor cell number in IgG multiple myeloma. *Journal of Clinical Investigation*, 49:11141121, 1970.
67. Anil Shanker, Michel Buferne, and Anne-Marie Schmitt-Verhulst. Cooperative action of CD8 T lymphocytes and natural killer cells controls tumour growth under conditions of restricted T-cell receptor diversity. *Immunology*, 129(1):41–54, 2010.
68. Anil Shanker, Grégory Verdeil, Michel Buferne, Else-Marit Inderberg-Suso, Denis Puthier, Florence Joly, Catherine Nguyen, Lee Leserman, Nathalie Auphan-Anezin, and Anne-Marie Schmitt-Verhulst. CD8 T cell help for innate antitumor immunity. *Journal of Immunology*, 179(10):6651–6662, 2007.
69. Ethan M Shevach, Richard A DiPaolo, John Andersson, Dong-Mei Zhao, Geoffrey L Stephens, and Angela M Thornton. The lifestyle of naturally occurring CD4+ CD25+ Foxp3+ regulatory T cells. *Immunological Reviews*, 212(1):60–73, 2006.
70. David R Shook and Dario Campana. Natural killer cell engineering for cellular therapy of cancer. *HLA*, 78(6):409–415, 2011.
71. Mark J Smyth, Michele WL Teng, Jeremy Swann, Konstantinos Kyparissoudis, Dale I Godfrey, and Yoshihiro Hayakawa. CD4+ CD25+ T regulatory cells suppress NK cell-mediated immunotherapy of cancer. *Journal of Immunology*, 176(3):1582–1587, 2006.
72. Eduardo D Sontag. A dynamic model of immune responses to antigen presentation predicts different regions of tumor or pathogen elimination. *Cell Systems*, 4(2):231–241, 2017.
73. NV Stepanova. Course of the immune reaction during the development of a malignant tumour. *Biophysics*, 24:917–923, 1980.

74. JW Stoop, BJM Zegers, PC Sander, and RE Ballieux. Serum immunoglobulin levels in healthy children and adults. *Clinical and Experimental Immunology*, 4(1):101, 1969.
75. H Suen, R Brown, S Yang, C Weatherburn, PJ Ho, N Woodland, N Nassif, P Barbaro, C Bryant, D Hart, et al. Multiple myeloma causes clonal T-cell immunosenescence: Identification of potential novel targets for promoting tumour immunity and implications for checkpoint blockade. *Leukemia*, 30(8):1716–1724, 2016.
76. Peter W Sullivan and Sydney E Salmon. Kinetics of tumor growth and regression in IgG multiple myeloma. *Journal of Clinical Investigation*, 51:16971708, 1972.
77. Can M Sungur, Yajarayma J Tang-Feldman, Erik Ames, Maite Alvarez, Mingyi Chen, Dan L Longo, Claire Pomeroy, and William J Murphy. Murine natural killer cell licensing and regulation by T regulatory cells in viral responses. *Proceedings of the National Academy of Sciences*, 110(18):7401–7406, 2013.
78. George W Swan and Thomas L Vincent. Optimal control analysis in the chemotherapy of IgG multiple myeloma. *Bulletin of Mathematical Biology*, 39(3):317–337, 1977.
79. Min Tang, Rui Zhao, Helgi van de Velde, Jennifer G Tross, Constantine Mitsiades, Suzanne Viselli, Rachel Neuwirth, Dixie-Lee Esseltine, Kenneth Anderson, Irene M Ghobrial, Jesús F San Miguel, Paul G Richardson, Michael H Tomasson, and Franziska Michor. Myeloma cell dynamics in response to treatment supports a model of hierarchical differentiation and clonal evolution. *Clinical Cancer Research*, 22(16):4206–4214, 2016.
80. Dat Q Tran. TGF-β: The sword, the wand, and the shield of FOXP3+ regulatory T cells. *Journal of Molecular Cell Biology*, 4(1):29–37, 2012.
81. Trisilowati, Scott W McCue, and Dann G Mallet. A cellular automata model to investigate immune cell-tumor cell interactions in growing tumors in two spatial dimensions. In Amina Eladaddi, Peter Kim, and Dann Mallet, editors, *Mathematical Models of Tumor-Immune System Dynamics*, volume 107 of *Springer Proceedings in Mathematics and Statistics*, pages 223–251. Springer, New York, 2014.
82. Marijke van der Giessen, Emmerentia Rossouw, T Algra van Veen, Erna van Loghem, BJ Zegers, and PC Sander. Quantification of IgG subclasses in sera of normal adults and healthy children between 4 and 12 years of age. *Clinical and Experimental Immunology*, 21(3):501, 1975.
83. Milica Vukmanovic-Stejic, Yan Zhang, Joanne E Cook, Jean M Fletcher, Arthur McQuaid, Joanne E Masters, Malcolm HA Rustin, Leonie S Taams, Peter CL Beverley, Derek C Macallan, et al. Human CD4+ CD25hi Foxp3+ regulatory T cells are derived by rapid turnover of memory populations in vivo. *Journal of Clinical Investigation*, 116(9):2423, 2006.
84. Yue-Jin Wen, Rui Min, Guido Tricot, Bart Barlogie, and Qing Yi. Tumor lysate-specific cytotoxic T lymphocytes in multiple myeloma: Promising effector cells for immunotherapy. *Blood*, 99(9):3280–3285, 2002.
85. Yan Zhang, Diana L Wallace, Catherine M De Lara, Hala Ghattas, Becca Asquith, Andrew Worth, George E Griffin, Graham P Taylor, David F Tough, Peter CL Beverley, and Derek C Macallan. In vivo kinetics of human natural killer cells: The effects of ageing and acute and chronic viral infection. *Immunology*, 121(2):258–265, 2007.